# X-ray absorption spectroscopy study of the local structures of crystalline Zn–In–Sn oxide thin films

D. E. Proffit,[1,a)] D. B. Buchholz,[1] R. P. H. Chang,[1] M. J. Bedzyk,[1] T. O. Mason,[1] and Q. Ma[2]

[1]*Department of Materials Science and Engineering, Northwestern University, Evanston, Illinois 60208, USA*
[2]*DND-CAT, Northwestern Synchrotron Research Center at Advanced Photon Source, Argonne, Illinois 60439, USA*

(Received 8 July 2009; accepted 14 October 2009; published online 10 December 2009)

The local structure of a Zn, Sn codoped $In_2O_3$ thin film grown on $\hat{c}$-plane sapphire by pulsed-laser deposition was examined by polarization-dependent x-ray absorption spectroscopy. The bixbyite film structure is both out-of-plane and in-plane oriented, and the structural results show that both Zn and Sn dopants occupy In sites. The In–O bond length is comparable to that in powder $In_2O_3$. However, both Sn–O and Zn–O bonds have two distinct distances in the first shell. Some of the Zn dopants are undercoordinated and, accordingly, some isovalent Sn dopants are overcoordinated for charge balance. In addition, the results suggest that the aliovalent Sn dopants form Frank–Köstlin clusters, $(2Sn_{In}^{\bullet}O_i'')^x$, which provide enough charge carriers to explain the Hall measurements.
 [doi:10.1063/1.3259385]

## I. INTRODUCTION

Transparent conducting oxides (TCOs) combine the contraindicated properties of high transparency and high conductivity, which make them useful as transparent electrodes in applications such as photovoltaics and light emitting displays. The current industry standard for TCOs is indium tin oxide (ITO).[1] Commercially available ITO films have high transparency in the visible region (>85%), high conductivities that can reach 10 000 S/cm, and are easily fabricated and etched.[2]

However, the increasing range of properties needed for emerging applications places demands on interfacial properties and materials compatibility. The limitations and cost of ITO have led to the development of alternate TCO materials, such as the Zn–In–Sn–O (ZITO) system. The discovery that up to 40% of indium in the indium oxide bixbyite structure can be codoped by zinc and tin has opened the door to development of this material as a low indium alternative to ITO.[3] The high doping level is attributed to the net isovalent substitution of indium by tin and zinc. An inherent Sn-rich off-stoichiometry enables persistent *n*-type conduction.[4] Frank and Köstlin[5] proposed the existence of neutral $(2Sn_{In}^{\bullet}O_i'')^x$ clusters, in which two tin donor atoms are compensated by an interstitial oxygen in ITO. Harvey *et al.*[6] suggested that the Frank–Köstlin (F-K) defect, $(2Sn_{In}^{\bullet}O_i'')^x$, may also occur in ZITO. The structural interstitial positions in $In_2O_3$ allow easy formation of these clusters. Addition or removal of oxygen from the neutral $(2Sn_{In}^{\bullet}O_i'')^x$ clusters results in large changes in the effective donor concentration and, therefore, also in the electron population and conductivity. Because the electron population depends on oxygen interstitials, the high temperature thermopower and conductivity will vary with a characteristic slope $(-1/8)$ when oxygen partial pressure varies within a certain regime.

The current challenge in optimizing these TCOs is to understand the relationship between their structure and optoelectronic properties and to establish their defect chemistry. Therefore, details of the local structures in ZITO materials are needed.[1] In this paper, we present a detailed structure analysis using x-ray absorption spectroscopy (XAS). In Sec. II, a general background of the XAS technique and the crystallographic details of $In_2O_3$ are given. In Sec. III, details on sample preparation, characterization, and XAS measurements are described. In Sec. IV, the local structure of a crystalline ZITO film is presented. In Sec. V, the physical properties of the film are discussed in terms of the structural details, and physical models are proposed.

## II. BACKGROUND

XAS is a powerful tool to investigate the local structure around a specific absorbing atom.[7] Analysis of the x-ray absorption near-edge structure (XANES) provides information about chemical state and site symmetry. Analysis of the extended x-ray absorption fine structure (EXAFS) provides information about interatomic distances, $R_i$, coordination numbers, $N_i$, statistical spread (root mean square) of the distances, $\sigma_i^2$, due to thermal motion and/or static disorder, and chemical species via characteristic backscattering amplitude, $|f_i(k)|$, and phase shift, $\varphi(k)$. The EXAFS spectrum is parameterized as[7]

$$\chi(k) = \sum_i \frac{N_i(\theta)|f_i(k)|S_0^2}{kR_i^2} \sin\left[2R_i k + \varphi(k) + \frac{2}{3}C_3 k^3\right] e^{-2R_i/\lambda(k)} e^{-2\sigma_i^2 k^2},$$

where $S_0^2$ is the intrinsic loss factor and $e^{-2Ri/\lambda(k)}$ is the attenuation factor due to the electron mean free path, $\lambda(k)$. Both are determined using a suitable reference material. $e^{-2\sigma_i^2 k^2}$ is the Debye–Waller factor. Note that $N_i$ is a function

[a)]Electronic mail: diana.proffit@gmail.com.

 

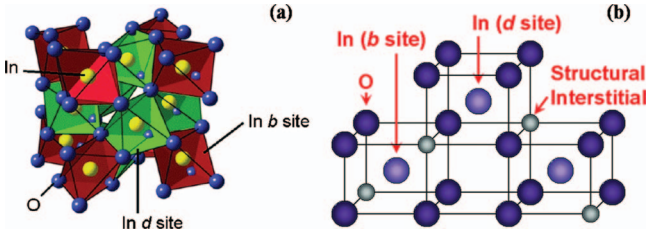


FIG. 1. (Color) (a) $In_2O_3$ bixbyite structure with octahedra marked (blue =oxygen atom and yellow=In atom). (b) Differing cation sites in the bixbyite structure shown without actual distortion.

of the angle $\theta$ between the probed chemical bond and synchrotron x-ray polarization direction. For *anisotropic* systems, say a textured film, probed at the $K$ absorption edge, $N_i = 3\Sigma_j^N \cos^2\theta$, whereas for *isotropic* systems $3\cos^2\theta \rightarrow 1$. $C_3$ is the EXAFS third cumulant, which accounts for the effect of anharmonic potential on the measured bond lengths. Through the Fourier transform of $\chi(k)$, one obtains the *pseudo-radial* distribution function ($p$-RDF) around the absorbing atom.

Indium oxide has the *bcc* bixbyite structure, which is the $C$-type rare-earth sesquioxide structure (space group Ia3, number 206).[8] It is described as the fluorite structure with one-quarter of the anions missing, resulting in so-called "structural vacancies," which are actually oxygen interstitial positions. The unit cell has a lattice constant of 10.117 Å and contains 80 atoms. Of the 32 cations, 8 (25%) sit on $b$-sites and 24 (75%) sit on $d$-sites. Each cation is surrounded by 6 oxygen atoms and 2 structural vacancy (interstitial) positions, as shown in Fig. 1. The $b$-site has the structural vacancies at two body-diagonal positions and 6 oxygen atoms equidistant from the cation position at 2.18 Å, whereas the $d$-site has the structural vacancies at two face-diagonal positions and 2 oxygen atoms each at 2.13, 2.19, and 2.23 Å. The coordination numbers of the first three shells are $N_1=N_2=N_3=6$.

The XAS data analyses were carried out using the ATHENA software package.[9] $S_0^2$, $N_i$, $R_i$, $\sigma_i^2$, and $C_3$ are all obtained by the FEFF8 simulations. $S_0^2$ for the powder ZnO reference is determined to be 0.93 based on the wurtzite structure, $S_0^2$ for powder $SnO_2$ is 1.04 based on the rutile structure, and $S_0^2$ for powder $In_2O_3$ is 1.03 based on the bixbyite structure.

## III. EXPERIMENTAL PROCEDURE

### A. Thin film preparation

A ZITO thin film was grown by pulsed-laser deposition (PLD) on a $\hat{c}$-plane sapphire substrate of $\sim 10\times 10$ mm$^2$. To achieve crystallinity, the substrate was resistively heated to 700 °C during deposition. A 248 nm KrF excimer laser was used with a 25 ns pulse duration operated at 2 Hz. The beam, which was focused to a $1\times 2$ mm$^2$ spot, delivered an energy of 200 mJ/pulse. The dense, hot-pressed, ceramic ZITO target had a metallic composition of 70.3 at. % In, 13.4 at. % Sn, and 16.3 at. % Zn. The partial pressure of oxygen during deposition was set to 15 mTorr in order to grow a film with a metallic composition of 78 at. % In, 12 at. % Sn, and 10 at. % Zn, i.e., $Zn_{0.20}In_{1.56}Sn_{0.24}O_3$. To prevent local heating, the target was rotated at 5 rpm and the laser beam was rastered. The target-substrate separation was fixed at 10 cm.

TABLE I. Composition and electrical data for ZITO thin film sample.

| Sample | Units | ZITO10/12 |
|---|---|---|
| Deposition temperature | °C | 700 |
| Pressure | mTorr | 15 |
| Substrate | | $\hat{c}$-sapphire |
| Thickness | nm | 180 |
| $\sigma$ | S/cm | 1565 |
| Hall mobility | cm$^2$/V s | 41.0 |
| $n$ | 1/cm$^3$ | $-2.4\times 10^{20}$ |
| In | | 78 |
| Sn | at. % | 12 |
| Zn | | 10 |

### B. Sample characterization

The compositions of the ZITO target and film were verified by energy dispersive x-ray analysis in a scanning electron microscope (Hitachi S4500). Multiple measurements of the ZITO target gave a standard deviation of 1 at. %. Sheet resistance, carrier type, area carrier concentration, and carrier mobility of the film were measured via a Hall measurement system (Bio-Rad Microscience LTD HL5500) in the Van der Pauw configuration with a 0.320 T field. The carrier density and resistivity were obtained by dividing the area carrier concentration and the sheet resistance by the film thickness, respectively. Film thickness was measured using a spectral reflectometer (Filmetrics F20). Table I shows the film growth conditions and physical properties. X-ray diffraction (XRD) measurements (Rigaku ATX-G Workstation) show that the film is oriented with $\langle 111\rangle$ normal to the sample surface and has no significant tilt. The $\omega$-scan of the {222} reflection indicates a 1.5% spread of the $d$ spacing. The in-plane XRD measurement indicates that the in-plane structure is somewhat oriented as well and has three-fold symmetry.

Synchrotron x-ray absorption measurements were carried out at the 5-BMD beamline of DND-CAT at the Advanced Photon Source (Argonne, IL). Spectra of the ZITO thin film, and reference samples of an $In_2O_3$ thin film and powder $In_2O_3$, $SnO_2$, and ZnO were collected around the Zn, In, and Sn $K$-edges, respectively. The powder reference samples were measured in transmission mode using the ionization chambers (Oxford-Danfysik). The powder was uniformly spread on Scotch tape (3M Corp.), which was folded to obtain a significant absorption signal ($\mu\Delta t \leq 1$). The reference and sample thin films were measured in fluorescence mode. The Zn-$K\alpha$, In-$K\alpha$, and Sn-$K\alpha$ fluorescence emissions were measured using a Canberra 13-element Ge solid state detector. The sample was mounted on a spinner and oriented vertically. Measurements were taken with the incident x-ray angle $\theta$ at about 6°, 30°, and 50° with respect to the sample surface.

## IV. LOCAL STRUCTURES OF THE ZITO FILM

The XANES spectra of the ZITO film together with the spectra collected on the reference materials are shown in Fig.

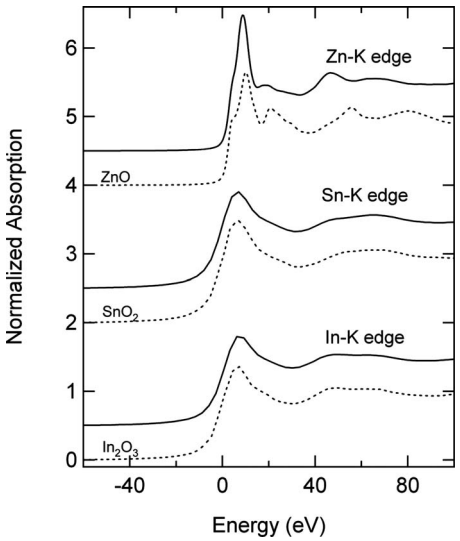


FIG. 2. Zn, In, and Sn *K*-edge XANES spectra of the film ZITO10/12 (solid lines) and of the reference materials (dotted lines) as labeled.

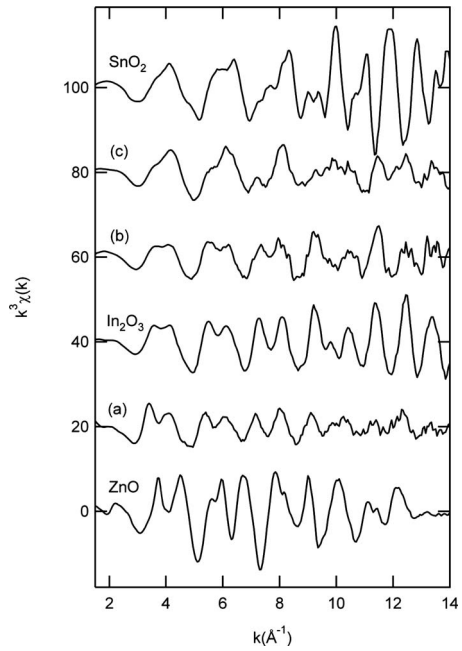


FIG. 3. EXAFS spectra of the ZITO film measured at (a) Zn *K*-edge, (b) In *K*-edge, and (c) Sn *K*-edge. The spectra of ZnO, $In_2O_3$, and $SnO_2$ are also presented.

2. XANES is sensitive to the chemical state and structural geometry of the absorbing atom.[7] The zero energy for the Zn *K*-edge spectra is referenced to the Zn *K*-edge of a metal Zn foil, while those for the In and Sn *K*-edges are referenced to powder $In_2O_3$ and $SnO_2$, respectively. The absorption edge positions measured from the sample all match well to their corresponding oxide references. This is a strong indication that the cations in the film have valences corresponding to the references of comparison, i.e., $Zn^{2+}$, $In^{3+}$, and $Sn^{4+}$.

The similarities among the In *K*-edge XANES and the Sn *K*-edge XANES are likely indicative of octahedral geometry around the In and Sn ions, as in bulk $In_2O_3$ and $SnO_2$. In contrast, the Zn *K*-edge XANES differs distinctly from that of wurtzite ZnO, which has Zn in tetrahedral coordination. Wang *et al.*[10] reported an x-ray absorption spectrum of goslarite, $ZnSO_4 \cdot 7H_2O$, in which Zn has an octahedral coordination. The Zn *K*-edge XANES of goslarite closely resembles that of the film, which suggests that the Zn ions in the film likely occupy octahedral In sites as well. Compared to the Zn *K*-edge XANES, the first intense transitions for In and Sn *K*-edges are broader due to the *1s* core hole lifetime effect.

Figure 3 shows the EXAFS spectra of the ZITO film and bulk ZnO, $In_2O_3$, and $SnO_2$. The In *K*-edge EXAFS spectrum (b) is similar to that of bulk $In_2O_3$, suggesting that the PLD-prepared film likely has the structure of bulk $In_2O_3$. However, both the Zn (a) and Sn (c) *K*-edge EXAFS spectra of the film differ from those of bulk ZnO and $SnO_2$ to various extents. For the Sn *K*-edge data, the low-*k* portion of the EXAFS data, due predominantly to lighter backscatters, is quite similar to that of bulk $SnO_2$, suggesting that the oxygen (first) coordination shell in the film is describable by that in $SnO_2$. The high-*k* portion of the EXAFS data ($k > 9$ Å) is very different from that of $SnO_2$. The differences between the Zn *K*-edge data of the film and bulk ZnO are quite obvious. In fact, the Zn (a) and Sn (c) *K*-edge spectra of the film better match that of $In_2O_3$. These qualitative analyses are consistent with the XANES observations, and further suggest that the local structures around both Zn and Sn in the film resemble that around In.

Figure 4 shows the *p*-RDFs for (a) the powder $In_2O_3$, $In_2O_3$ film, and the ZITO film obtained from the In *K*-edge data, (b) the powder $SnO_2$ and the ZITO film obtained from the Sn *K*-edge data, and (c) the powder ZnO and the ZITO film obtained from the Zn *K*-edge data. Also shown in the figure are the results (dashed lines) of the FEFF8 simulations based on the structure centered on the *b*-site cation in the bixbyite structure. As can be seen, the local structure around

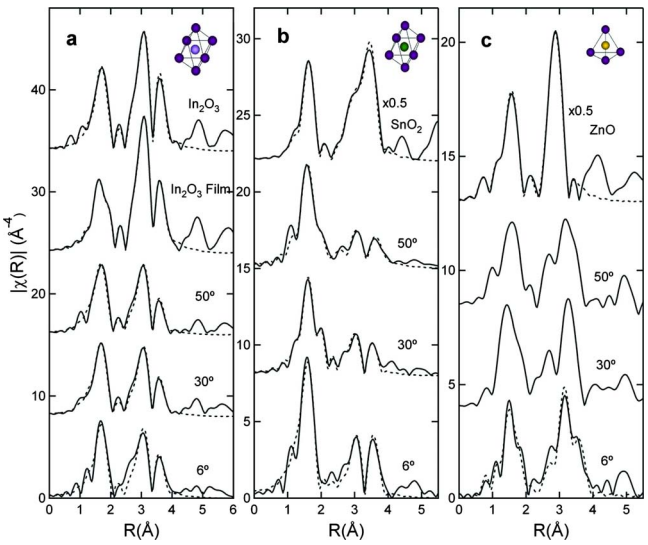


FIG. 4. (Color online) The *p*-RDFs (solid lines) and corresponding FEFF8 simulation results (dashed lines) based on the absorber at the *b*-site are shown for the (a) In *K*-edge, (b) Sn *K*-edge, and (c) Zn *K*-edge. All sample edges and reference film and powders are shown. Local structural units of the reference powders are also displayed (octahedron vs tetrahedron).

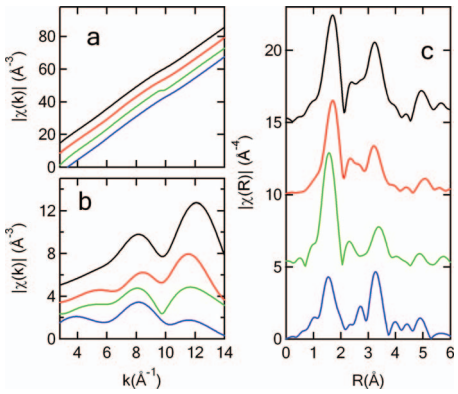


FIG. 5. (Color) [(a) and (b)] Phases and amplitudes extracted from the *p*-RDFs in the *R*-range from 2.4 to 4 Å (see Fig. 3). (c) The *p*-RDFs are obtained by using the spectra in $k=\sim 3-10.6$ Å$^{-1}$. The curves are vertically displaced for clarity. Black line: powder $In_2O_3$, red line: In *K*-edge, green line: Sn *K*-edge, and blue line: Zn *K*-edge for the film.

indium in the ZITO film is similar to that of bulk $In_2O_3$. Unlike that of powder $In_2O_3$, the first peak of the $In_2O_3$ film consists of two In–O bond distances, as indicated by the shoulder. The Sn *K*-edge *p*-RDF is very different from that of bulk $SnO_2$, in particular, for the structure beyond the first shell, which is consistent with the *k*-space observation discussed above. In addition, the first coordination shell splits into two components when measured at a larger incident angle, which probes more in-plane structure. The overall structure around Sn, in fact, very much resembles that around In, except that the structures of high shells are more attenuated.

The Zn *K*-edge *p*-RDF is also very different from that of bulk ZnO, and thus excludes the wurtzite structure. The first peak consists of more than one distance. There is a prominent kink at $k\sim 10$ Å$^{-1}$ in the phase (not shown), indicating a separation of ~0.16 Å ($\Delta R=\pi/2k$).[11] For the ZITO film, the apparent differences in the *R*-range from 2.4 to 4 Å between the Zn *K*-edge *p*-RDFs and those from the In and Sn *K*-edges may result from the structure, the large elemental differences between Zn–In (or –Sn) and In–In (or –Sn), or both. Comparison of the phases [Fig. 5(a)] and amplitudes [Fig. 5(b)] extracted from the *p*-RDFs in this *R*-range reveals good agreement in phase among the three *K*-edge spectra. The dips in amplitude near 6 Å$^{-1}$ are characteristic for heavier backscatters such as In and Sn. The dips near 10 Å$^{-1}$ may be due predominantly to the interference between single scattering events from In or Sn atoms at two different distances such as 3.35 and 3.82 Å ($\Delta R=0.47$ Å) in the case of bulk $In_2O_3$. The Fourier transforms of the spectra from ~3 to ~10.6 Å$^{-1}$ give quite similar *p*-RDFs for all the spectra [Fig. 5(c)]. Therefore, in addition to some differences in the interatomic distances, the apparent differences in the *p*-RDFs in this *R*-range are due in part to changes in the spectral weight. The local structure around Zn may be quite similar to that around In and Sn in the film.

Due to the qualitative analyses presented above, a cluster based on the bixbyite structure with a radius of 6 Å is constructed to center around either In, Sn, or Zn. The FEFF8 simulations are carried out with the appropriate $S_0^2$ values (see Sec. II). Simulation results (see Fig. 4) are obtained using the data between $k=3.2-13.2$ Å$^{-1}$ and $R=1.0-4.1$ Å. It is seen that the bixbyite structure reproduced well the film spectra. Table II lists the *R*, *N*, and $\sigma^2$ of the first coordination shells for the films and bulk $In_2O_3$. The error bars are estimated from the results obtained under various conditions such as using the data in various *R*-ranges and *k*-ranges, and, in particular, the error bars for distances cover those results obtained from simulations including the $C_3$ term.

For the $In_2O_3$ film In *K*-edge data and the ZITO film Sn *K*-edge data measured at $\theta=30°$ and $\theta=50°$, the splitting in the first shells can be well accounted for by assuming two bond distances. Likewise, the attempt to simulate the Zn–O peak by assuming two distances yields a good fit at 2.00 and 2.17 Å. However, the coordination numbers obtained from this simulation are not reliable, because these two components have a phase shift of about $\pi$. One way to evaluate such a situation is to use the shorter *k*-range data so that the peak splitting is not resolved, which allows the assumption of a single broad distribution. The Zn *K*-edge results shown in Table II are obtained in this way.

The splitting of the first shell in the case of the $In_2O_3$ film cannot be explained by disorder at the *d*-site, because this splitting is not resolved in the powder $In_2O_3$, which contains 75% *d*-sites [see Fig. 4(a)]. The likely cause of this splitting is a somewhat larger disorder around the In atoms in the film. A similar effect may be expected in the ZITO film, since both the $In_2O_3$ and ZITO films were grown under similar conditions. However, other than a slight increase in the

TABLE II. Structural parameters obtained for the first coordination shell.

| Sample | | $R_{M-O}$ (Å)[b] | $N(\theta)$ 6° | 30° | 50° | | $\sigma_2$ (Å$^2$) |
|---|---|---|---|---|---|---|---|
| *$In_2O_3$ powder*[a] | | *2.16 (±0.02)* | | *6.0* | | | *0.0056* |
| $In_2O_3$ film | | 2.09/2.22 | 6.2 | | | (±0.3) | 0.0062[c] |
| ZITO | In *K*-edge | 2.17 (±0.03) | 4.9 | 5.9 | 6.1 | (±0.3) | 0.0050–0.0074 |
| | Sn *K*-edge | 2.08/2.25 | 6.3/0 | 3.1/2.6 | 4.0/1.8 | (±0.4) | 0.0060, 0.0090[c] |
| | Zn *K*-edge[d] | 2.04–2.18 | 4.7 | 4.7 | 5.0 | (±0.3) | 0.0140–0.0160 |

[a]The polycrystalline data collected in transmission mode.
[b]Error bars and the range on distances include the $C_3$ effect.
[c]These $\sigma^2$ values include two components.
[d]The results are obtained using the data for $k=3.1-10$ Å$^{-1}$.

Debye–Waller factors (see Table II), the first shell structure around the In atoms in the ZITO film is not as disordered as in the $In_2O_3$ film; the shoulder on the second peak in the *p*-RDF measured at $\theta=6°$ is enhanced [see Fig. 4(a)]. In contrast, the local structures around the Sn and Zn atoms show rather pronounced anisotropy, and the splitting of the bond distances is clearly seen when the data are measured at certain angles [see Figs. 4(b) and 4(c)]. The longer Sn–O bond has a bias toward the in-plane orientation and the same is somewhat true for the longer Zn–O bond.

The first shell distortion around Sn and Zn clearly has some bearing on the second shell attenuation, particularly for the structure around Sn. It is therefore not surprising that the simulation using a cluster centered on the *d*-site yielded much improved simulation of these structures (results not shown). Instead of the two unique second shell distances at the *b*-site, the *d*-site has four distances in the second shell.

## V. DISCUSSION

The local structures of the $Zn_{0.20}In_{1.56}Sn_{0.24}O_3$ film are described through detailed XAS analyses. Strong evidence is presented that in the ZITO film, both Sn and Zn substitute for indium in a structural framework similar to the bixbyite structure of bulk $In_2O_3$. The first coordination shell around the In atom can be well described by a single In–O bond length that is comparable to that in bulk $In_2O_3$ (2.18 Å).[8] However, the first coordination shells around Sn and Zn split into two components. Both $[SnO_6]$ and $[ZnO_x]$ appear to orient in a similar fashion such that the longer bonds lie in the plane. The first shell split around Sn may be understood by a mechanism similar to the Jahn–Teller distortion. For a single bond length, a $[SnO_6]$ unit with either $R_{Sn-O}=2.08$ or 2.25 placed into the $In_2O_3$ matrix will induce a large volume change of about 12% on average $[\Delta V/V=3(\Delta R/R)]$. A large restoring energy will build up $(\text{stress}\propto\Delta V/V)$, which can only be relieved by rearrangement of the atoms. Probably by no accident, the average Sn–O bond length is 2.16 Å, or the weighted average Sn–O bond length is 2.13–2.16 Å for the data measured at 30° and 50°. A similar argument should readily apply to the $[ZnO_x]$ structure.

The coordination number around the In atom shows an angular dependence (see Table II), and the orientation effect can play a role in this. For instance, $N(\theta)$ is calculated to be as small as 3.99 and as large as 6.67 along the [111] direction, depending on which site is considered, in a *perfect* bixbyite structure. Compared to this range, the effect of orientation is much less in the ZITO film, which may by itself reveal that the structural orientation of the ZITO film is far from perfect. The coordination number around Sn also shows some angular dependence. However, instead of $N(\theta)$ also being relatively small along [111], it is significantly larger than that around In. Overcoordinated Sn atoms in ITO samples have been reported, and thus it is quite likely that this large number around Sn may, in fact, be due to overcoordination.[12] The coordination number around Zn does not seem to vary, which may indicate that disorder around Zn plays a role in diminishing the polarization effect $(3\cos^2\theta\rightarrow 1)$. This also implies that some, if not all, Zn atoms are indeed undercoordinated in the ZITO film.

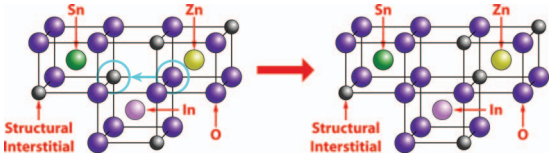


FIG. 6. (Color) Schematic of a structural rearrangement of oxygen in ZITO from Zn to Sn, with Sn and Zn on *d*-sites.

An undercoordinated Zn and an overcoordinated Sn can be explained quite well by an oxygen arrangement, depicted in Fig. 6, which does not change either the stoichiometry or the charge balance of the material. An oxygen anion sits on an interstitial site around Sn, creating a vacancy around Zn. Accordingly, the neighboring In site is now a disordered *d*-site, which may *in part* compensate the energy cost of this arrangement. The vacancies, at least most of them, around Zn are likely not caused by substoichiometry. Otherwise, the charge carrier concentration $(n=2[V_O^{\bullet\bullet}])$, assuming that oxygen substoichiometry produces charge carriers, would be $6.2\times10^{21}$ cm$^{-3}$, which is inconsistent with $n=2.4\times10^{20}$ cm$^{-3}$ from the Hall measurement. X-ray photoelectron spectroscopy measurements also confirm a stoichiometric film at the surface of the film.

Confirmation that an *extra* oxygen resides on an interstitial site in the Sn first nearest neighbor shell may be also sought from other works. There are two types of Sn in ZITO, as proposed by Harvey *et al.*:[4] isovalent species, or Sn that is compensated by Zn, and excess aliovalent species, or Sn that is uncompensated. There is strong evidence that the aliovalent Sn ions form F-K defects, just as they do in ITO. Harvey *et al.*[13] measured the conductivity and thermopower of ZITO under varying oxygen partial pressures at high temperature, and the resulting plot of log(conductivity) versus $\log(pO_2)$ showed the characteristic slope of $-1/8$, which is associated with F-K defects. This characteristic slope has been verified by the confirmation of F-K defects in ITO through a combination of experiments and calculations, including EXAFS, time-of-flight neutron diffraction, density functional theory calculations, and the abovementioned high temperature conductivity/thermopower measurements as a function of varying oxygen partial pressure.[12] Assuming that all uncompensated Sn ions, which make up 2% of the total cations, form reduced F-K clusters, the calculated charge carrier concentration is $3.2\times10^{20}$ cm$^{-3}$. This value matches well with the measured charge carrier concentration $2.4\times10^{20}$ cm$^{-3}$ and, thus, supports the idea that the aliovalent Sn is most likely overcoordinated.

In addition, the undercoordination of Zn suggests that compensated Sn may also be overcoordinated. According to the Zn:Sn ratio, the $N(=5)$ value for Zn implies that, at most, 90% of the compensated Sn can be overcoordinated, assuming that all the oxygen atoms leaving Zn go to Sn. This scenario requires that $N=6.8$ for Sn, which would result in a coordination number for Sn that is larger than for In when measuring along the [111] direction and which may be close to the upper boundary coordination number calculated for a single crystal, as mentioned above. This is consistent with

the experimental results (see Table II). Therefore, some, if not most, compensated Sn is likely overcoordinated as well.

## VI. CONCLUSIONS

XAS measurements reveal the details of the local structure of the $Zn_{0.20}In_{1.56}Sn_{0.24}O_3$ film. The results show that the crystalline ZITO film structure can be described based on bulk $In_2O_3$. Ample evidence indicates that In, Sn, and Zn are present in octahedral coordination and that Sn and Zn are therefore substitutional dopants on the In sites of the bixbyite structure. The first coordination shell around the In has a single In–O bond length of 2.17 Å, which is comparable to that in bulk $In_2O_3$. However, the first coordination shells around Sn and Zn have two distances whose average is close to that of the In–O bond distance. Codoping of Sn and Zn appears to create a local strain around these dopants in the film.

Consideration of the coordination numbers with respect to the structure results above, the measured charge carrier concentration, charge balance, and previous experiments provides enough evidence to propose a structural model. Although the measured coordination numbers are convoluted due to angular dependence resulting from the effects of x-ray polarization and film orientation, the Zn appears undercoordinated ($N \sim 5$) and the Sn overcoordinated ($N > 6$). This suggests that oxygen vacancies tend to form around Zn, which are compensated by oxygen interstitials around isovalent Sn species, and that aliovalent (uncompensated) Sn species form Frank–Köstlin clusters, $(2Sn_{In}^{\bullet}O_i'')^x$. The composition dependence of the film structure is the subject of future study and will be addressed in a forthcoming discussion.

## ACKNOWLEDGMENTS

This work is supported in part by the NSF MRSEC program at Northwestern University under Grant No. DMR-0520513 (D.B.B., R.P.H.C., M.J.B., and T.O.M.) and in part by the U.S. Department of Energy under Grant No. DE-FG02-08ER46536 (D.B.B., R.P.H.C., and T.O.M.). D.E.P. acknowledges the support of a NSF Graduate Research Fellowship. DND-CAT is supported by the E.I. DuPont de Nemours & Co., The Dow Chemical Co., the NSF via Grant No. DMR-9304725 (M.J.B. and Q.M.), and the State of Illinois via Grant No. IBHE HECA NWU 96. The APS is supported by the DOE via Contract No. DE-AC02-06CH11357. The authors acknowledge helpful discussions with K. R. Poeppelmeier and C. A. Hoel.

[1] D. S. Ginley and C. Bright, MRS Bull. **25**, 15 (2000).
[2] B. G. Lewis and D. C. Paine, MRS Bull. **25**, 22 (2000).
[3] G. B. Palmer, K. R. Poeppelmeier, and T. O. Mason, Chem. Mater. **9**, 3121 (1997).
[4] S. P. Harvey, T. O. Mason, D. B. Buchholz, R. P. H. Chang, C. Körber, and A. Klein, J. Am. Ceram. Soc. **91**, 467 (2008).
[5] G. Frank and H. Köstlin, Appl. Phys. A: Mater. Sci. Process. **27**, 197 (1982).
[6] S. P. Harvey, T. O. Mason, Y. Gassenbauer, R. Schafranek, and A. Klein, J. Phys. D **39**, 3959 (2006).
[7] J. J. Rehr and R. C. Albers, Rev. Mod. Phys. **72**, 621 (2000).
[8] M. Marezio, Acta Crystallogr. **20**, 723 (1966).
[9] B. Ravel and M. Newville, J. Synchrotron Radiat. **12**, 537 (2005).
[10] Y. Wang, A. Li, Y. Zhan, L. Wei, Y. Li, G. Zhang, Y. Xie, J. Zhang, Y. Zhang, and Z. Shan, J. Radioanal. Nucl. Chem. **273**, 247 (2007).
[11] D. T. Jiang, E. D. Crozier, and B. Heinrich, Phys. Rev. B **44**, 6401 (1991).
[12] G. B. Gonzalez, T. O. Mason, J. P. Quintana, O. Warschkow, D. E. Ellis, J. H. Hwang, J. P. Hodges, and J. D. Jorgensen, J. Appl. Phys. **96**, 3912 (2004).
[13] S. P. Harvey, *Surface and Bulk Electronic Structure of Bixbyite Transparent Conducting Oxides* (Materials Science and Engineering, Northwestern University, Evanston, IL, 2008), p. 220.